Constraints on charged black holes from merger-ringdown signals in GWTC-3 and prospects for the Einstein Telescope

Hua-Peng Gu,[1,2] Hai-Tian Wang,[1,2,*] and Lijing Shao[2,3,†]

[1]Department of Astronomy, School of Physics, Peking University, Beijing 100871, China
[2]Kavli Institute for Astronomy and Astrophysics, Peking University, Beijing 100871, China
[3]National Astronomical Observatories, Chinese Academy of Sciences, Beijing 100012, China

(Received 16 October 2023; accepted 10 January 2024; published 30 January 2024)

Whether astrophysical black holes (BHs) can have charge is a question to be addressed by observations. In the era of gravitational wave (GW) astronomy, one can constrain the charge of a merged BH remnant using the merger-ringdown signal of the GW data. Extending earlier studies, we analyze five GW events in GWTC-3, assuming Kerr-Newman BHs. Our results show no strong evidence for a charged BH, and give a limit on the charge-to-mass-ratio $Q < 0.37$ at 90% credible level. Due to the charge-spin degeneracy in the waveform and the limited signal-to-noise ratios, it is challenging for LIGO/Virgo/KAGRA observations to provide better constraints. We further simulate data for the Einstein Telescope, where signal-to-noise ratios can be as large as ∼270 in the ringdown signal. These simulated events allow us to consider the 220, 221, and 330 ringdown modes altogether, which can help break the charge-spin degeneracy. The analysis of a simulated GW150914-like signal shows that the Einstein Telescope can improve the constraints on the charge-to-mass-ratio to $Q \lesssim 0.2$ at 90% credible level with one ringdown signal.

DOI: 10.1103/PhysRevD.109.024058

I. INTRODUCTION

The existence of black holes (BHs), as predicted by Einstein's general relativity (GR), has been substantiated through a series of observations [1,2]. These astronomical observations not only empirically elucidate the physical attributes of BHs but also serve as a robust platform for validating different BH models and theories of gravity. With the groundbreaking detection of the gravitational wave (GW) event GW150914 by the LIGO/Virgo collaboration [3], GW astronomy has emerged as a potent tool for probing the properties of BHs. Recent observations by the LIGO/Virgo/KAGRA (LVK) collaboration have achieved signal-to-noise ratios (SNRs) as high as 26 for binary BH (BBH) merger events [4]. Looking ahead, next-generation GW observatories like the Einstein Telescope (ET) [5] are anticipated to reach SNRs exceeding 200 for BBH mergers, thereby enabling even more precise measurements of BH properties [6–8].

In the context of GR, the most general solution for a stationary, asymptotically flat BH is the Kerr-Newman (KN) BH, characterized by mass, spin, and charge [9,10]. However, astrophysical BHs are generally considered to be Kerr-like, as they are expected to be electrically neutral due to decharging effects from their surrounding environment. To illustrate this, consider a toy model of a BH with mass M and charge $+q_M$, surrounded by particles of mass m and charge $\pm q_m$. If the BH charge is sufficiently large such that, with $G = 1$ in Gaussian units,

$$q_M q_m > Mm, \tag{1}$$

then the electromagnetic force will dominate over gravity, causing the BH to attract only negatively charged particles. Consequently, the BH will become neutralized on a timescale far shorter than the timescale associated with GWs [11–13]. Moreover, even in the vacuum, processes like vacuum polarization and pair production contribute to the neutralization of the BH [14]. The upper limit for the charge-to-mass ratio of a BH has been estimated to be

$$Q \equiv q_M/M \lesssim 10^{-5}\frac{M}{M_\odot}, \tag{2}$$

thereby reinforcing the Kerr hypothesis for BHs [15].

Empirical evidence lends credence to the theoretical premises discussed above. For instance, observations of the bremsstrahlung surface brightness decay in the Galactic central BH, Sgr A*, suggest that its charge-to-mass ratio is less than 10^{-18} [16,17]. Since the discharge mechanisms mentioned above apply for all BHs regardless of their mass, all the astrophysical BHs should have negligible charge. It is worth noting that the term "charge" in this context refers exclusively to the electromagnetic charge. Before we only talked about the electric charge, while the BHs may carry

*Corresponding author: wanght@pku.edu.cn
†Corresponding author: lshao@pku.edu.cn

magnetic charge by primordial magnetic monopoles [18]. The electric and magnetic charges are indistinguishable for a perturbed BH in vacuum [19–21]. However, theories extending beyond the Standard Model or GR permit BHs to carry different kinds of charges (see, e.g., Ref. [22]). The foregoing analysis, for example, relies on the high charge-to-mass ratio of electrons. In contrast, the minicharged dark matter model, predicated on an additional hidden $U(1)$ gauge field, could give rise to particles with lower charge-to-mass ratios, thereby making charged BHs less constrained [15,23]. Moreover, certain modified gravity theories also admit the possibility of BHs carrying specific kinds of charges, which would influence the metric and yield observable effects. As such, direct observations of the metric offer a model-independent avenue for testing these theories.

Nonetheless, conventional methods for constraining the BH charge via metric measurements in its vicinity tend to yield rather weak limits. For instance, the Event Horizon Telescope's recent imaging of Sgr A* has established an upper bound of 0.72 for the charge-to-mass ratio at a 68% credible level (CL) [24–27]. More stringent constraints can be garnered from GW detectors, particularly in the context of BBH mergers. In such events, the GW signal during both the inspiral and ringdown phases serves as a probe of BH properties pre- and postmerger, respectively. Our analysis is primarily concerned with the latter. At the ringdown stage, the GW signal manifests as a composite of damped sinusoids, known as quasinormal modes (QNMs) [28]. Both the oscillation frequency and damping time of these QNMs are dependent on the attributes of the resultant merged BH, including its charge. By extracting QNM frequencies from the ringdown data, one can deduce the parameters characterizing the QNM spectrum—a technique commonly referred to as BH spectroscopy [29,30].

There are three primary challenges associated with constraining the charge of the resultant BH using GW detectors. The first challenge pertains to the computation of QNMs for KN BHs. The interplay between electromagnetic and gravitational perturbations complicates the analytical derivation of QNM frequencies for KN BHs [31,32]. Initial perturbative solutions for KN BH QNMs were first obtained by Pani *et al.* [33,34] in the slow-rotation limit, by Mark *et al.* [35] under the weakly charged condition, and by Zimmerman and Mark [36] for extremal KN BHs. Wang *et al.* [37] later employed geodesic correspondence to approximate KN QNMs in the eikonal limit. This approximation constrains the charge-to-mass ratio of the BH remnant in GW150914 to be less than 0.38 at 90% CL, while this result made an ansatz for QNMs at high values of the charge. Moreover, numerical solutions, especially for certain dominant QNMs have been calculated by Dias *et al.* [38–40]. For the inspiral stage, however, a complete KN solution remains elusive. Existing studies have primarily focused on numerical simulations at some certain limits, such as for low charge-to-mass ratios [19,41–44]. Consequently, a comprehensive inspiral-merger-ringdown (IMR) signal analysis for KN BHs is currently unfeasible [45]. The second challenge arises from the limited sensitivity of existing GW detectors. Even for high-confidence events like GW150914, the SNRs for postmerger data barely exceed 10 [46]. This limitation hampers our ability to extract higher-order QNMs from the ringdown data. When only dominant modes are considered, the charge and spin parameters become strongly degenerate, rendering precise constraints on the BH remnant's charge impracticable. The third challenge pertains to data analysis of ringdown signals, including the determination of the start time of the ringdown signal. In this work, following previous studies [37,46–48], we assume that it starts from the peak amplitude when including the first overtone mode.

The GW Transient Catalog (GWTC) provides a compendium of GW events observed by the LVK collaboration [49–51]. This dataset has been extensively employed in various BH analyses, including tests of GR and its modifications. Prior analyses have rigorously measured parameters such as the mass and spin of the remnant BHs, providing a basis for validating subsequent model-dependent studies [47,52,53]. In testing GR, the working model is typically Kerr-like, and, to date, no significant deviations from GR have been observed. Carullo *et al.* [46] leveraged the merger-ringdown signals from the GWTC-2 dataset [50] to constrain the charge of remnant BHs. Utilizing numerical solutions for dominant QNMs from Dias *et al.* [39,40], they performed a KN BH analysis and derived the charge-spin distribution for several high-confidence GW events. A prior based on previous IMR analyses of Kerr BHs was also applied to further constrain the remnant BH charge. Their most stringent constraint on the charge-to-mass ratio is less than 0.33 at 90% CL for GW150914. Building upon this work, we employ GWTC-3 data [51] to scrutinize the charge of remnant BHs in five high-credibility GW events. Our results show negative Bayes factors between the KN and Kerr model. Consequently, our analysis does not strongly support the existence of charged BH remnants. Due to the low SNRs in ringdown data, coupled with charge-spin degeneracy, the error margins in our analysis are substantial even with the improved noise levels in current LVK observations. Although our constraints are substantially weaker than those derived from electromagnetic observations, which can be on the order of $Q \sim 10^{-18}$, our approach is complementary, and offers the advantage of being model independent.

Moreover, to assess the potential for detecting BH charges with the future GW detector ET, we conduct analyses using simulated GW data. Designed to achieve a tenfold increase in sensitivity [5], ET has not yet been constructed, but simulated data analyses can offer valuable insights into future constraints on remnant BH charges

using merger-ringdown signals. Enhanced detector sensitivity not only reduces the uncertainty in our results but also enables us to include higher-order QNMs in the template, thereby mitigating the charge-spin degeneracy. In this study, we generate merger-ringdown waveforms based on the Kerr BH model and inject them into noise simulated from ET's designed power spectral density. Subsequent analyses indicate that the constraint on BH charge could be tightened to $Q < 0.2$ at the 90% CL.

The remainder of this paper is organized as follows. In Sec. II, we introduce the Bayesian framework for constraining BH charge. Section III presents our findings derived from GWTC-3 data, confirming the charge-spin degeneracy of the remnant BH. In Sec. IV, we discuss results based on simulated ET ringdown data, specifically addressing how the inclusion of higher multipole modes can alleviate charge-spin degeneracy and yield more stringent constraints on BH charge. Conclusions and discussions are provided in Sec. V.

II. METHOD

In this section, we outline the waveform model and the GW data employed for Bayesian inference.

During the ringdown phase, the GW signal emanates from the oscillations of the remnant BH. In the context of a Kerr BH, the metric tensor field can be decomposed into a background field and a perturbation term. This perturbation term is a superposition of a set of eigenfunctions, leading to the solutions known as QNMs [54,55]. Each QNM is characterized by a damped sinusoid with a complex frequency,

$$\tilde{\omega}_{\ell mn} \equiv \omega_{\ell mn} - i\gamma_{\ell mn}, \quad \gamma_{\ell mn} = \frac{1}{\tau_{\ell mn}}, \tag{3}$$

where $\omega_{\ell mn}$ represents the oscillating frequency, $\gamma_{\ell mn}$ denotes the damping frequency, and $\tau_{\ell mn}$ is the damping time. Each QNM is distinguished by three indices, including ℓ and m, which arise from the angular eigenfunctions, and n, referred to as the overtone number that is associated with the damping time. Generally, higher overtone modes exhibit more rapid damping [56].

In the case of a KN BH, electromagnetic perturbations come into play, intertwining with gravitational perturbations. The specific calculations for this are intricate and fall beyond the scope of this paper. As posited by the no-hair theorem [57], the QNM frequencies are fully determined by the mass M, dimensionless spin a, and charge-to-mass ratio Q of the remnant BH, expressed as

$$\tilde{\omega}_{\ell mn} = \tilde{\omega}_{\ell mn}(M, a, Q). \tag{4}$$

Here, we adopt the convention where a represents the dimensionless spin and Q signifies the charge-to-mass ratio q/M. Without losing generality, we assume that a and Q are non-negative. Both a and Q are constrained to lie between 0 and 1, subject to a GR-based constraint

$$a^2 + Q^2 \leq 1. \tag{5}$$

For the precise form of Eq. (4), we rely on the numerical solutions provided by Dias *et al.* [39,40]. To elaborate further, Carullo *et al.* [46] used an analytical fit for the numerical solutions [39,40] and listed the fitting coefficients in their appendix. In this work we use their analytical fitting results.

GW signal during the ringdown phase constitutes a superposition of various possible QNMs. Typically, the $\ell = 2, m = 2, n = 0$ mode (hereafter referred to as the 220 mode) serves as the dominant contributor to the ringdown signal [4,58,59]. The 221 mode, characterized by a similar oscillating frequency but a shorter damping time, has also been considered in some previous QNM fittings for Kerr BHs [58,60]. Additionally, Capano *et al.* [61] reported evidence supporting the existence of the 330 mode, while analyses of Siegel *et al.* [62] support the existence of 210 and 320 modes when including precessing degrees of freedom. The disagreements are mainly between the remnant mass and spin of these two different ringdown analyses. Since Dias *et al.* [39,40] only provided the numerical solutions for the 220, 221, and 330 modes, we remain considering 220, 221, and 330 modes in our KN analysis. The higher modes, despite their theoretical underpinning [63], remain elusive in current LVK observations due to limited detector sensitivity. Consequently, the template we employ for QNM fitting is

$$\begin{aligned} h^+(t) - ih^\times(t) = {} & A_{220} e^{-i(\tilde{\omega}_{220}(t-t_0)+\varphi_{220})}\, {}_{-2}S_{220}(\iota, \varphi) \\ & + A_{221} e^{-i(\tilde{\omega}_{221}(t-t_0)+\varphi_{221})}\, {}_{-2}S_{221}(\iota, \varphi) \\ & + A_{330} e^{-i(\tilde{\omega}_{330}(t-t_0)+\varphi_{330})}\, {}_{-2}S_{330}(\iota, \varphi), \end{aligned} \tag{6}$$

where ${}_{-2}S_{\ell mn}$ represents the spheroidal harmonics [64], which depend on the spin polar angle ι and the spin azimuthal angle φ, and t_0 is the reference start time for the postmerger. The real amplitude $A_{\ell mn}$ and phase $\varphi_{\ell mn}$ of each mode are treated as free parameters. In Eq. (6) we do not consider the contribution of the counterrotating modes with the negative m (see Refs. [46,65–67]). In addition we assume a nonprecessing symmetry. Moreover, the polarization angle ψ and the orientation of the GW event must also be specified to convert the observed GW data into h^+ and $h^\times$ components [56]. In summary, the parameters utilized for QNM fitting include

$$\{M, a, Q, A_{\ell mn}, \varphi_{\ell mn}, \iota, \psi\}. \tag{7}$$

In this formulation, the spin azimuthal angle φ is subsumed into the phase $\varphi_{\ell mn}$. Also, for our work based on the GWTC-3 data, we adopt the values of the sky location and

start time reported in Ref. [68] for these events, so that they are not included in Eq. (7). Specifically, following Abbott *et al.* [47], we use a reference time t_0 computed from an estimate of the peak of the strain, $\sqrt{h_+^2 + h_\times^2}$, from the full IMR analyses.

The prevailing model for GW data analysis is based on Kerr-like BHs, premised on the expectation that BHs are electromagnetically neutral. Nonetheless, even when focusing solely on ringdown data, introducing charge as an additional parameter yields results comparable to those from the Kerr BH model. This arises from the strong degeneracy between the spin and charge of the remnant BH, allowing the effects of spin to be partially offset by an appropriate charge component (as elaborated in Sec. III). Consequently, spin estimates from prior analyses employing the Kerr BH model can be interpreted as a form of "effective spin" if there is a nonvanishing charge. Employing a KN BH model for data fitting allows us to derive charge distributions for the remnant, thereby establishing upper limits on its charge. The constraints obtained are model independent and serve to rule out scenarios involving highly charged remnants, although the emergence of charge in these KN fits is most likely an artifact of charge-spin degeneracy.

Building upon the GWTC-2 dataset, which includes credible GW events up to the O3a observing run of the LVK collaboration, Carullo *et al.* [46] examined the potential influence of charge in the merger-ringdown signals. Their analysis revealed the presence of charge-spin degeneracy and also included a "null test." In this test, they assumed the validity of the Kerr hypothesis and incorporated a Kerr BH prior for the final spin and mass, based on previous IMR results. Utilizing the derived posterior distributions of charge, an upper limit of $Q < 0.33$ for GW150914 at the 90% CL was obtained.

In the present study, we focus on five events cataloged in GWTC-3: GW191109, GW191222, GW200129, GW200224, and GW200311. These events have been specifically discussed in Ref. [47] due to their credible ringdown signals. The parameters of their remnant BHs are well constrained relative to the prior, and the Bayesian evidence supports the existence of a signal over mere Gaussian noise. Furthermore, the sky-frame orientations of these events have been accurately determined. For these five events, the LVK collaboration [47] provided the outcomes of Kerr BH analyses, which serve as the foundation for our subsequent analyses.

Our analysis of KN BHs employs the PYRING software package, a time-domain Bayesian inference tool designed for analyzing ringdown signals [4,58,59,69]. The sampling method that we utilized is the *CPNest* algorithm [70], which estimates the evidence and obtains the posterior distribution iteratively. For our KN BH analysis, we initially set uniform priors for M, $A_{\ell mn}$, $\cos\iota$, $\varphi_{\ell mn}$, and ψ as indicated in Eq. (7). Specifically, M is chosen in the range of $[0, 200]M_\odot$, $A_{\ell mn}$ is chosen in the range of $[0, 10] \times 10^{-21}$, $\cos\iota$ is chosen in the range of $[-1, 1]$, and both $\varphi_{\ell mn}$ and ψ in the range $[0, 2\pi]$. The parameters a and Q are uniformly distributed within the quarter disc defined by $a^2 + Q^2 \leq 1$, $a \geq 0$, and $Q \geq 0$. Following Ref. [47], we assume fixed values for the sky location and the start time.

The posterior distribution of these parameters is then computed using Bayes' theorem

$$p(\vec{\theta}|d, \mathcal{H}) = \frac{p(\vec{\theta}|\mathcal{H}) \cdot p(d|\vec{\theta}, \mathcal{H})}{p(d|\mathcal{H})}, \tag{8}$$

where $\vec{\theta}$ represents the model parameters, d is the observed data, and $\mathcal{H}$ denotes the model. Here, $p(d|\mathcal{H})$ is the evidence, calculated iteratively via CPNEST [71]. This evidence is instrumental for model comparison, expressed through the Bayes factor when comparing model 1 and model 2,

$$\mathcal{B}_1^2 = \frac{p(d|\mathcal{H}_2)}{p(d|\mathcal{H}_1)} = \frac{\int p(d|\vec{\theta_2}, \mathcal{H}_2) p(\vec{\theta_2}|\mathcal{H}_2) \mathrm{d}\vec{\theta_2}}{\int p(d|\vec{\theta_1}, \mathcal{H}_1) p(\vec{\theta_1}|\mathcal{H}_1) \mathrm{d}\vec{\theta_1}}. \tag{9}$$

For the GWTC-3 ringdown data, we incorporate both the 220 and 221 modes into our model. Given that the 330 mode is considerably weaker and usually falls below the noise level of LVK detectors, it is excluded from our KN analysis. In the Kerr model analysis, Abbott *et al.* [47] did not find preference for the 330 mode in the five GWTC-3 events that are used in this work. Our analysis employs ringdown data sampled at a rate of 16 kHz, which surpasses the commonly used 4 kHz rate. We utilize 0.4 s of data following the merger for autocorrelation function estimation to extract the signal, and the full 32 s of data to estimate the power spectral density. To estimate the SNR, ρ, of a signal $h(t)$, we have

$$\rho^2 = h(t) \mathcal{C}^{-1} h(t)^\intercal, \tag{10}$$

where $\mathcal{C}$ is the autocovariance matrix, which is the Toeplitz form of the autocorrelation function.

III. RESULTS FROM GWTC-3

In this section, we delineate the outcomes of our KN BH analysis for the five GW events selected from GWTC-3. A central aspect of our discussion will revolve around the phenomenon of charge-spin degeneracy.

Differently from the approach taken by Carullo *et al.* [46], our analysis employs a sampling rate of 16 kHz. Figure 1 displays the charge-spin distribution we obtained for the remnant BH of GW150914. The 90% credible region (CR) in our findings closely aligns with early work [46], while our result shows a slightly narrower distribution mainly due to the 16 kHz sampling rate. Employing the

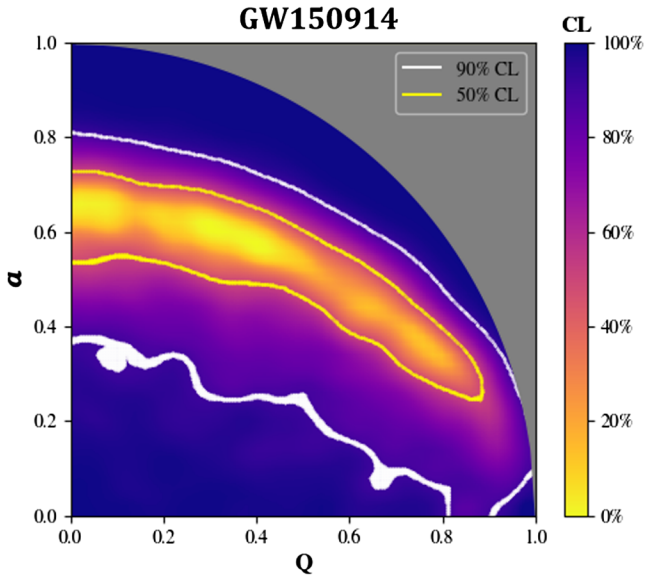

FIG. 1. Charge-spin posterior distribution for GW150914. Different colors signify varying CLs within the distribution. The 90% CR and 50% CR are demarcated by white and yellow lines, respectively. The gray region violates the constraint $a^2 + Q^2 \leq 1$. Note that the mass parameter exhibits minimal correlation with the charge and is thus not displayed.

same methodology, we establish an upper limit on the remnant BH charge of $Q < 0.35$ at 90% CL. Further, in the $Q \to 0$ limit, the final spin approximates 0.67, aligning with IMR results based on the Kerr BH model. The final mass, although not depicted in the figure, also concurs with these Kerr-based IMR outcomes. Subsequent analyses are performed on the selected events from GWTC-3.

Figure 2 presents the charge-spin distributions of the remnant BHs for the five events featured in GWTC-3. Among them, GW200129 and GW200224 yield more stringent constraints on both charge and spin, while GW191222 and GW200311 offer weaker constraints due to their relatively low ringdown SNRs. Intriguingly, the most stringent yet puzzling constraints emanate from GW191109. Although there exists a strong correlation between charge and spin for this event, the constraint on charge is surprisingly lax. No discernible improvement in SNR accounts for this anomaly (see Table I). The ringdown SNR for GW191109 is 12.6, comparable to that of GW150914. We will delve into this particular case in further detail later.

To assess the validity of our KN BH model, we concurrently perform analyses under the assumption of the Kerr hypothesis, setting the charge to zero. Subsequently, we compute the Bayes factor between the KN and Kerr BH models as outlined in Eq. (9). The results indicate a slight preference for the Kerr BH model, as most of the log Bayes factors are negative (see Table I). This outcome aligns with similar findings from GWTC-2 events [46], lending support to the prevailing Kerr hypothesis that remnant BHs are uncharged.

The charge-spin distribution for GW191109 exhibits a "beltlike" shape, a stark contrast to the more diffuse distributions typically observed. This unique formation is a direct consequence of the charge-spin degeneracy, wherein various points in the charge-spin parameter space yield indistinguishable QNM frequencies, thus forming a beltlike distribution in the results. Although this phenomenon is also manifest in the other four events, it remains less conspicuous due to the larger associated uncertainties.

Notably, our ringdown analysis for GW191109 reveals a discrepancy when compared to previous IMR results in the Kerr BH model. The IMR result for GW191109 gives $M_f = 132.7^{+21.9}_{-13.8} M_\odot$ and $a_f = 0.60^{+0.22}_{-0.19}$. However, in the $Q \to 0$ limit, our analysis yields $M_f = 184^{+12}_{-12} M_\odot$ and $a_f = 0.85^{+0.05}_{-0.06}$. These findings align with the ringdown analysis by the LVK collaboration [47], where the Kerr BH model was employed to fit the ringdown signal, resulting in $M_f = 179.0^{+23.7}_{-21.7}$ and $a_f = 0.81^{+0.08}_{-0.14}$ at 90% CL. This discordance between the ringdown and inspiral signals points to an inconsistency, an issue also noted in Ref. [47], where they attributed it to the non-Gaussian noise. For the remaining four events, our ringdown-derived results are consistent with earlier IMR analyses.

We now delve into the charge-spin degeneracy alluded to earlier, extending the preliminary discussion by Carullo *et al.* [46]. Figure 3 vividly illustrates how the QNM frequencies vary with both the final spin a and charge Q, based on the analytical fit results from Carullo *et al.* [46]. Specifically, the dimensionless frequencies $M\omega$ and $M\tau^{-1}$ serve as functions of the dimensionless spin a and charge-to-mass ratio Q. As depicted in Fig. 3, the oscillating and damping frequencies of the 220 mode exhibit a strikingly similar dependence on a and Q, giving rise to the beltlike distribution in the Q-a plane.

Introducing additional QNMs into the fitting—such as the 221 and 330 modes—can alleviate this degeneracy. As Fig. 3 reveals, different damping frequencies manifest distinct dependencies on a and Q. The inclusion of higher modes enriches the information available for a and Q estimation, thereby yielding more precise constraints. However, due to the limited sensitivity of current LVK observations, accurate extraction of these higher modes remains challenging. In our analysis based on GWTC-3 data, we confined ourselves to the 220 and 221 modes, resulting in pronounced degeneracy. Next-generation GW detectors like the ET are expected to facilitate the inclusion of higher modes in the models, thereby breaking the degeneracy more effectively. Additionally, it is worth noting that this degeneracy is intrinsic for small Q values, as the frequencies have weak dependence on Q when Q is near zero [39,40]. This implies that BHs with minimal charge may evade detection through this method, setting a lower bound on the charge constraints.

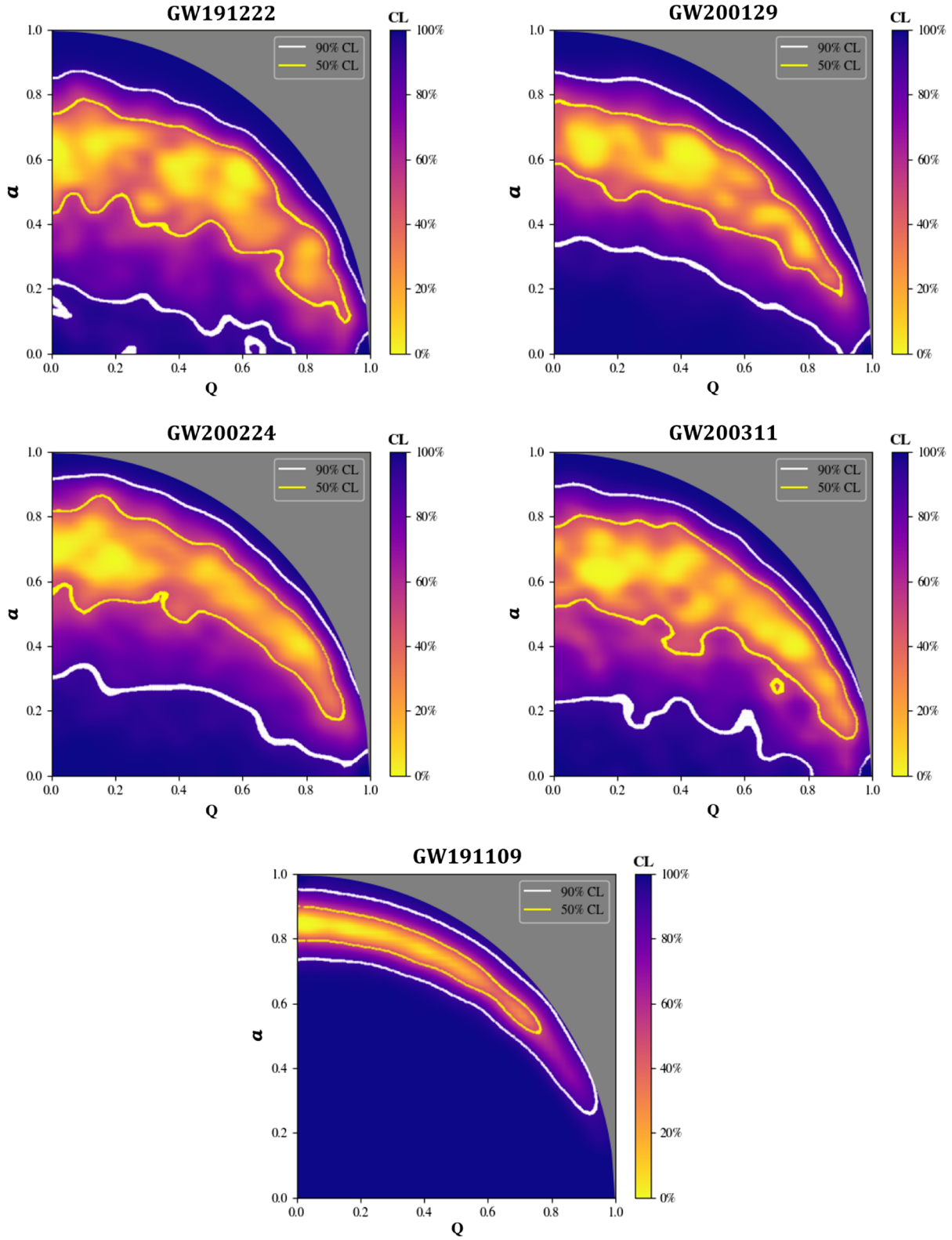

FIG. 2. Same as Fig. 1, but for GW191222, GW200129, GW200224, GW200311, and GW191109.

TABLE I. Constraints on BH charges, denoted by $Q_{\max}$, for five GWTC-3 events and two GWTC-2 events, given at the 90% CL for both Gaussian IMR and flat bounded IMR priors. Also listed are the logarithmic Bayes factors between the KN BH and Kerr BH models, denoted by $\ln \mathcal{B}^{\mathrm{KN}}_{\mathrm{Kerr}}$, for both the uniform prior and IMR prior cases (null tests), as well as the SNRs for the ringdown data (calculated also from PYRING).

Event	$Q_{\max}$ (Gaussian prior)	$Q_{\max}$ (flat bounded prior)	$\ln \mathcal{B}^{\mathrm{KN}}_{\mathrm{Kerr}}$	$\ln \mathcal{B}^{\mathrm{KN}}_{\mathrm{Kerr}}$ (null)	Ringdown SNR
GW191109	0.77	⋯	−1.4	−0.5	12.6
GW191222	0.50	0.59	0.3	−0.4	6.4
GW200129	0.37	0.45	0.3	−0.6	13.0
GW200224	0.37	0.53	−1.1	−0.7	10.7
GW200311	0.47	0.57	−0.8	−0.5	7.9
GW150914	0.37	0.35	−0.6	−0.7	12.6
GW190521_07	0.40	0.41	−0.2	−0.8	9.6

The charge and spin are correlated in the above results. To obtain more stringent constraints on the charge of the remnant BH, we can constrain the spin first. Since our method is based on the Bayesian inference, we could apply a more stringent prior on the spin. Since the electromagnetic observations [16,17] support the Kerr hypothesis, a tentative choice is to use the final spin result from IMR analysis, which is based on the Kerr BH model. This procedure, i.e., using the Kerr prior to obtain the posterior distribution of charge, is called the "null test" in Carullo *et al.* [46], as this prior is based on the hypothesis that the final BH does not possess charge. Among the obtained posterior distributions of charge, all the events except GW191109 show a decreasing probability density from $Q = 0$, signifying that they are very likely to have negligible charge. GW191109, however, has a very broad charge distribution. This is due to the strong correlation of charge and spin, where they cannot be well constrained at the same time. These results are shown in Fig. 4. The results of GW150914 and GW190521_07 (i.e., GW190521_074359) are also presented for comparison. Here we choose the form of the priors as Gaussian, instead of the flat bounded prior used by Carullo *et al.* [46]. We chose a Gaussian prior because it matches the distribution of the parameters from IMR analysis more accurately. However, from another point of view, the Gaussian prior will introduce more information compared to a uniform distribution. Furthermore, the final spin distribution of GW191109 from Kerr ringdown analysis falls outside the range of its IMR result, which makes it unsuitable to adopt a flat bounded prior. We choose the value of the priors according to the results of the LVK collaboration [47].

We use the 90% CL limit in the posterior charge distributions as the upper bound on charge, for the selected events separately. The upper limits on charge are listed in Table I, where we also show the limits given by flat bounded prior for comparison. For results of GWTC-3, GW200129, and GW200224 give the strongest constraint $Q < 0.37$. This constraint is at the same level as the GWTC-2 results from Carullo *et al.* [46]. GW191222 and GW200311 have lower ringdown SNRs and can only give limits at about $Q < 0.5$. GW191109 gives the worst constraint in our selected GWTC-3 events. One may argue that this is due to the discrepancy between the IMR Kerr prior and KN results for GW191109; i.e., we choose a prior smaller than its Kerr spin from ringdown analysis, and the charge-spin degeneracy causes the nonzero value of charge (the charge is fitted to compensate for the spin), thus leading to this broad distribution. However, as will be shown in the following, this is not related to the choice of prior.

Constraints here are based on the IMR-based prior and KN BH model. We choose this prior according to the Kerr BH hypothesis. To assess the validity of this assumption, we perform a companion analysis using the Kerr BH model and compare the results with those obtained using the KN BH model. In both situations, we adopt the Kerr prior (i.e., IMR-based prior). Figure 5 presents the posterior distributions of the remnant mass and spin for the five GW events under consideration. For all events, except GW191109, the obtained remnant mass and spin are visually identical for the two models. The spin posterior is larger in the Kerr case because of the degeneracy between the final mass and final spin. The spin distribution in the Kerr BH model may be slightly higher than that in the KN BH model, which can be attributed to the charge-spin degeneracy. We also compute the evidence for the Kerr BH model and calculate the Bayes factors for the null test. The log Bayes factors are all negative in our results, suggesting that the Kerr model provides a slightly better fit to the data. However, it should be noted that these values are quite small, indicating that a charged BH cannot be ruled out. These results are also summarized in Table. I.

For GW191109, the spin obtained from the Kerr BH model is notably higher than the spin obtained from the KN BH model. In both cases, we adopt the IMR Kerr prior, implying that the observed difference is not a result of prior selection but rather originates from the intrinsic differences between the Kerr BH and KN BH models. On the other hand, the distribution of the spin is larger in the Kerr case, which is due to the degeneracy between the final mass and final spin. This may simply be an effect of charge-spin degeneracy. Furthermore, GW191109 is a unique event, whose results are very likely influenced by its intrinsic

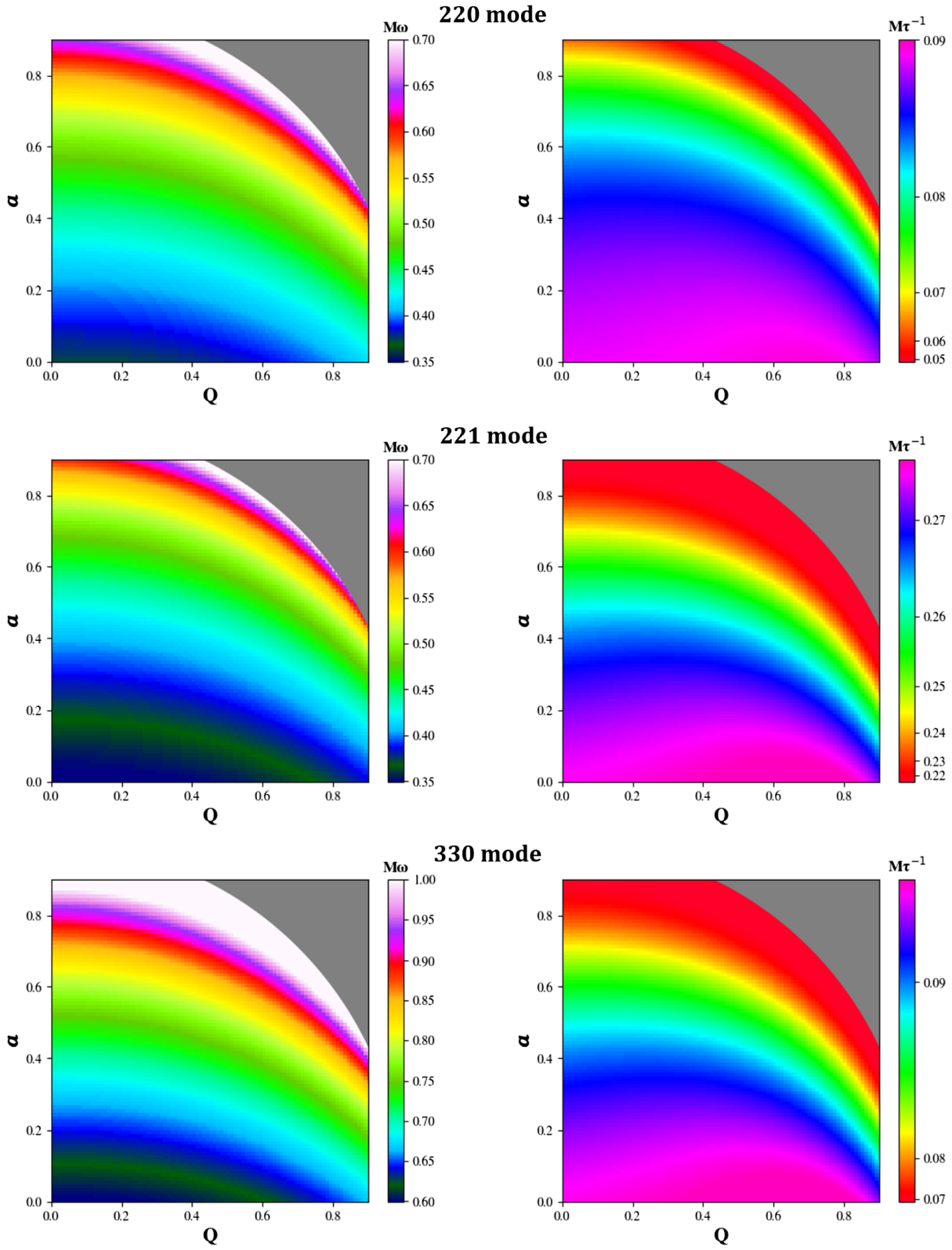

FIG. 3. QNM frequencies for the 220, 221, and 330 modes. The left panels display the oscillating frequencies, while the right panels show the damping frequencies. Different colors signify different frequency values. The gray region violates the constraint $a^2 + Q^2 \leq 1$.

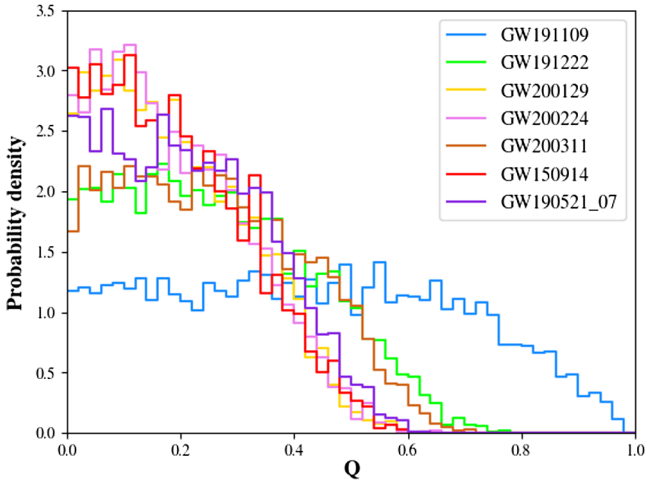

FIG. 4. Constraints on the final BH charge, according to the Gaussian prior of spin from Kerr IMR analysis. Different lines represent the posterior charge distributions of different events.

noises. The logarithmic Bayes factor for this event is −0.5, suggesting that the KN result is not strong. Consequently, we are inclined to attribute the discrepancy in the final spin between the Kerr BH and KN BH models to the non-Gaussian noise, rather than the presence of charge.

IV. ET SIMULATION

The charge-spin degeneracy prevents us from giving stronger constraints on the BH charge. To break the degeneracy, as illustrated in Sec. III, incorporating higher QNMs might be a solution. However, the requirement to detect higher modes places higher demands on the SNR of the ringdown signal. Therefore, in this section, we analyze the simulated GW ringdown data, using the noise of ET. ET is one of the next-generation GW observatories planned for construction in the 2030s. Designed as an equilateral triangle with arms extending 10 km, ET aims for a tenfold enhancement relative to LVK detectors in sensitivity, thereby paving the way for more precise QNM analyses [72].

To begin, we simulate the ringdown waveform using parameters that mirror those of the GW150914 event, with $M_f = 68.0M_\odot$, $a_f = 0.67$, and the polarization angle $\psi = 0.0$. We incorporate three QNMs—220, 221, and 330—with amplitude levels consistent with the GW150914 signal. In the Kerr BH framework, we set the amplitude ratios $A_{220} = 2.0$, $A_{221} = 3.0$, and $A_{330} = 0.2$, guided by theoretical values that relate the 22 ($l = 2$, $m = 2$) and 33 modes [73].[1] Subsequently, we embed this simulated waveform into the Gaussian noise spectrum of ET. The ET noise spectrum used in our study is provided by *GWToolbox* [74].[2] The SNR for our simulated event approximates 270.

We proceed with Bayesian inference using the KN BH model on the simulated ET ringdown data, employing a methodology consistent with our earlier approach. The only modification is the inclusion of an additional higher mode, specifically the 330 mode, in the fitting procedure. The resulting charge-spin distribution is depicted in the left panel of Fig. 6. The posterior distribution for charge predominantly converges toward zero. When juxtaposed with the GWTC-3 results, the error margins are markedly reduced, and the correlation between Q and a is more discernible. However, the beltlike distribution persists, indicating that the charge-spin degeneracy is not entirely eliminated, and the degeneracy is noticeably lessened.

We further investigate the impact of incorporating higher modes into our analysis. As delineated in Sec. III, the inclusion of higher modes can mitigate the charge-spin degeneracy. We now focus on the extent of this effect in incorporating the 330 mode, apart from the improvement in SNR. The right panel of Fig. 6 shows the outcome when considering only the 220 and 221 modes, under the KN BH model for the simulated ringdown signal. Compared to the left panel, where the 220, 221, and 330 modes are all included in the fitting, adding the 330 mode exhibits slightly weaker degeneracy effects. Although we anticipate that even more precise results could be achieved by including still higher modes like the 440 mode, the requisite QNMs for the KN BH model remain to be computed.

We proceed to replicate the foregoing analysis using the Kerr BH model and also compute the Bayes factor $\mathcal{B}^{\mathrm{KN}}_{\mathrm{Kerr}}$. The logarithm of the Bayes factor amounts to −0.6, signaling a preference for the Kerr BH model over the KN BH model. Given that the signal was simulated under the assumption of the Kerr BH model, this outcome aligns with our expectation. However, the presence of charge-spin degeneracy raises the question of whether the Kerr BH model would still yield a reasonable fit even if the actual signal had included a nonzero charge. To scrutinize this, we inject ringdown signals with charges $Q = 0.2$ and $Q = 0.4$. The log Bayes factors, although small, are positive in both cases, validating the robustness of our analysis. The negative log Bayes factor emerges only when the BH is not substantially charged, underscoring the utility of the Bayes factor in evaluating the Kerr hypothesis in future ET observations. The differences between these Bayes factors would be more significant when incorporating higher QNMs, where the above illustration could be more informative. These findings are summarized in Table II.

[1]Although the relative amplitude for the 221 mode is not theoretically determined in Ref. [73], we adopt our own fitting results from GW150914. Specifically, the maximum likelihood set of values yielded a ratio of $A_{220}: A_{221} = 2:2.9$. This approximate ratio was further corroborated by our GWTC-3 analysis for all events.

[2]http://www.gw-universe.org/.

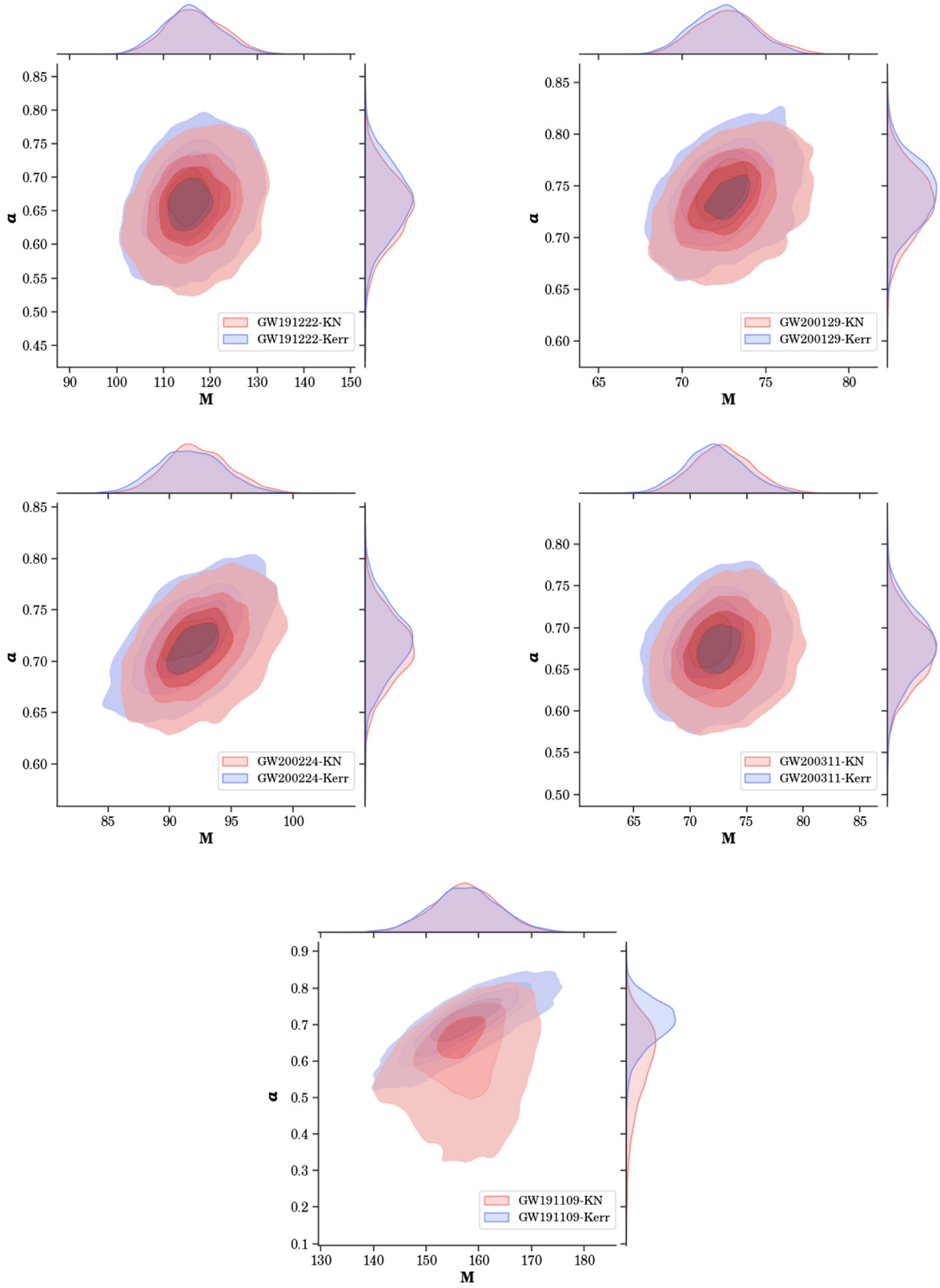

FIG. 5. Distributions of final mass M (in the unit of $M_\odot$) and final spin a for five GWTC-3 events, under the Kerr IMR prior. The blue and red shadows represent the probability density distributions in the Kerr BH model and in the KN BH model, respectively. The top and right panels display the projected distributions of final mass and final spin.

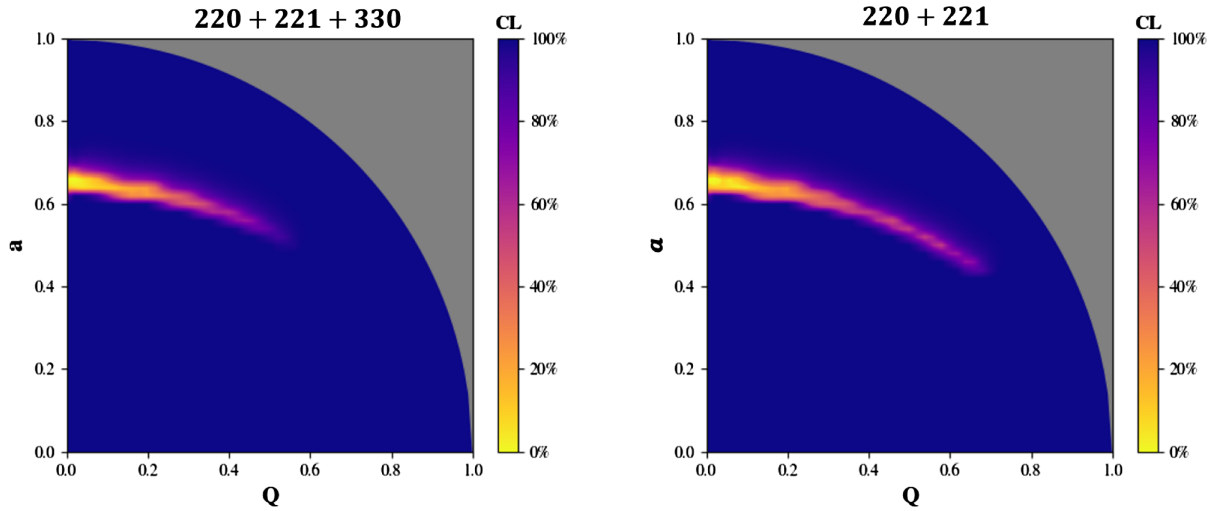

FIG. 6. Same as Fig. 1, but for the simulated ET ringdown data, where the injected final spin and the final charge of the remnant are $a = 0.67$ and $Q = 0$, respectively. The left panel presents the posterior when incorporating the 220, 221, and 330 modes collectively. In comparison, the right panel is for only considering 220 and 221 modes.

We next turn our attention to the so-called null test, in which we employ Kerr-based priors to constrain the final spin and evaluate the upper limits on the remnant charge. The priors used for the remnant mass and spin are outlined in Table II, along with the derived posterior distributions for the remnant charge. In addition to the Kerr BH scenario, we also examine cases with injected charges $Q = 0.2$ and $Q = 0.4$ for comparative analysis. As depicted in Fig. 7, these cases yield noticeably distinct charge distributions, even when the priors are rooted in the Kerr hypothesis. This outcome signals that the charge-spin degeneracy is only partially alleviated. For the $Q = 0$ case, we constrain the remnant charge to $Q < 0.2$ at the 90% CL. If only considering the 220 and 221 modes, the constraint is about $Q < 0.3$ at 90% CL, which is at the same level as the GWTC-3 outcomes.

Our constraint of $Q < 0.2$ on the remnant charge may appear somewhat modest, especially when contrasted with existing LVK constraints, $Q \lesssim 0.3$, despite the tenfold enhancement in ET's sensitivity. Cardoso *et al.* [15] theorized that more stringent constraints could be achieved for high-spin events. Confirming this, our simulation with $a = 0.9$ yielded an upper limit of $Q < 0.15$. However, this tighter constraint may in part be attributed to the $a^2 + Q^2 \leq 1$ restriction. Indeed, our simulation results fall short of the predictions made by Cardoso *et al.* [15], who posited an upper limit on Q of less than 0.1. We attribute this discrepancy to the differing methodologies. Different from the employed Fisher information matrix approach with a fixed spin in Cardoso *et al.* [15], our Bayesian analysis contends with the inherent degeneracy between spin and charge, making the results more realistic. Simulations with higher SNRs did not significantly alter these charge constraints, suggesting that including additional QNMs in the ringdown model is crucial to obtaining more robust limits.

TABLE II. Fitting results for simulated ringdown signals with varying remnant charges. The columns represent the injected remnant charge Q, the logarithm of the Bayes factor between the KN and Kerr BH models $\ln \mathcal{B}^{\mathrm{KN}}_{\mathrm{Kerr}}$, the prior for the final mass and spin utilized in the null test at the 90% CL,[a] the posterior distribution of charge at the 1-σ level in the null test and the SNRs for the simulated data.

Injected Q	$\ln \mathcal{B}^{\mathrm{KN}}_{\mathrm{Kerr}}$	Kerr mass ($M_\odot$)	Kerr spin	Posterior Q (null)	Ringdown SNR
0.0	−0.6	$68.7^{+0.5}_{-0.6}$	$0.670^{+0.015}_{-0.015}$	$0.09^{+0.05}_{-0.09}$	267.8
0.2	0.2	$68.3^{+0.7}_{-0.7}$	$0.682^{+0.017}_{-0.019}$	$0.17^{+0.10}_{-0.12}$	268.9
0.4	0.7	$67.3^{+0.5}_{-0.5}$	$0.719^{+0.012}_{-0.012}$	$0.24^{+0.13}_{-0.09}$	274.7

[a]In actual scenarios, the priors for mass and spin would be determined by IMR analysis. However, as we have not simulated the inspiral phase, we employ the Kerr BH fitting results for this ringdown signal as a surrogate prior. Though this approach lacks strict Bayesian rigor, it serves as a reasonable approximation for the $Q = 0.2$ and $Q = 0.4$ cases.

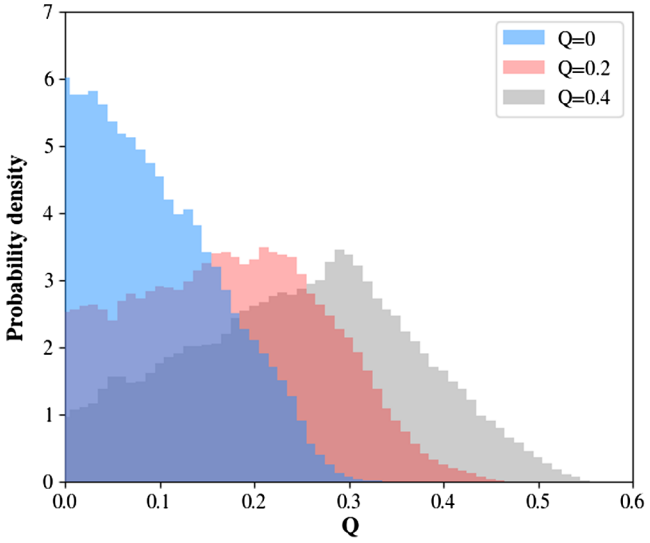

FIG. 7. Posterior distributions of the final BH charge for the simulated ET ringdown data using the Kerr prior. The blue, red, and gray shadows represent the results with an injected remnant charge $Q = 0$, $Q = 0.2$, and $Q = 0.4$, respectively.

V. CONCLUSIONS

In this study, our primary focus has been on constraining the charge of remnant BHs using merger-ringdown GW data from GWTC-3 and simulated data from the ET. We computed the posterior distributions for both charge and spin of the remnant BHs. While our constraints from GWTC-3 data echoed previous findings, the simulated ET data offered enhanced constraints. However, the overarching challenge remains the degeneracy between charge and spin.

From the GWTC-3 dataset, we zeroed in on five events that exhibited trustworthy ringdown signals. In our QNM analysis, we took into account both the 220 and 221 modes, deriving distributions for charge and spin of the resultant BHs. Notably, these distributions are heavily influenced by the charge-spin degeneracy. This is particularly evident in the case of GW191109, which displayed a pronounced correlation between remnant charge and spin, resulting in a distinctive beltlike distribution in the charge-spin plane. Upon employing a Kerr-based prior informed by preceding IMR analyses, constraints such as $Q < 0.37$ emerged from single events like GW200129 and GW200224, aligning closely with findings from GWTC-2. Our subsequent evaluations of the Kerr hypothesis suggest that most events exhibit charges consistent with zero, though the case for GW191109 remains somewhat ambiguous. Given the prevailing charge-spin degeneracy and the current limitations in the sensitivity of detectors, all computed Bayes factors between the KN BH and Kerr BH models are negative. Although the Kerr BH model performs better in describing the five selected GW events, it is still insufficient to exclude the KN model.

In our ET simulation, we generated synthetic ET data for BHs with varying remnant charges. Given the elevated SNRs achievable with ET, we were able to include 220, 221, and 330 modes in our analysis, thereby ameliorating the charge-spin degeneracy issue to some extent. Consequently, the posterior distributions for charge and spin improved substantially, manifesting significantly reduced errors. However, complete elimination of charge-spin degeneracy remains elusive, as evidenced by the persistence of beltlike distributions in our results. Our simulation validated the efficacy of Bayes factors in scrutinizing the Kerr hypothesis in the context of ET data. Furthermore, the upper limit on charge obtained from the "null test" improved to $Q < 0.2$ for $a \approx 0.67$ and $Q < 0.15$ for $a \approx 0.9$ with ET.

The crux of our investigation has been the persistent appearance of the charge-spin degeneracy. This phenomenon stems from the similar dependencies of currently utilized QNMs on both remnant charge and spin. The inclusion of additional QNMs in future analyses could potentially alleviate this degeneracy, thereby sharpening constraints on BH charge and facilitating more accurate identification of charged remnant BHs. Given that ET provides the capability to probe higher QNMs, future work will require expanded calculations on higher KN QNMs. Finally, if there are some mechanism resulting in similar charge-to-mass ratios for remnant BHs, one may also consider to perform event stacking in order to obtain tighter constraints on the BH charge. Nevertheless, such stacking relies on extra assumptions and is less general than the constraints from single events as obtained in this work.

ACKNOWLEDGMENTS

We thank Gregorio Carullo, Harrison Siegel, and the anonymous referee for helpful comments. This work was supported by the National Natural Science Foundation of China (Grants No. 11975027, No. 12247152, No. 11991053, and No. 11721303), the China Postdoctoral Science Foundation (Grant No. 2022TQ0011), the National SKA Program of China (Grant No. 2020SKA0120300), the Max Planck Partner Group Program funded by the Max Planck Society, and the High-performance Computing Platform of Peking University. H. T. W. is supported by the Opening Foundation of TianQin Research Center. LIGO Laboratory and Advanced LIGO are funded by the United States National Science Foundation (NSF) as well as the Science and Technology Facilities Council (STFC) of the United Kingdom, the Max-Planck-Society (MPS), and the State of Niedersachsen/Germany for support of the construction of Advanced LIGO and construction and operation of the GEO600 detector. Additional support for Advanced LIGO was provided by the Australian Research Council. Virgo is funded, through the European Gravitational Observatory (EGO), by the French Centre National de Recherche Scientifique (CNRS), the Italian Istituto Nazionale di

Fisica Nucleare (INFN) and the Dutch Nikhef, with contributions by institutions from Belgium, Germany, Greece, Hungary, Ireland, Japan, Monaco, Poland, Portugal, Spain. K. A. G. R. A. is supported by Ministry of Education, Culture, Sports, Science and Technology (MEXT), Japan Society for the Promotion of Science (JSPS) in Japan; National Research Foundation (NRF) and Ministry of Science and ICT (MSIT) in Korea; Academia Sinica (AS) and National Science and Technology Council (NSTC) in Taiwan of China.

[1] R. A. Remillard and J. E. McClintock, Annu. Rev. Astron. Astrophys. **44**, 49 (2006).
[2] K. Akiyama *et al.* (Event Horizon Telescope Collaboration), Astrophys. J. Lett. **875**, L1 (2019).
[3] B. P. Abbott *et al.* (LIGO Scientific and Virgo Collaborations), Phys. Rev. Lett. **116**, 061102 (2016).
[4] B. P. Abbott *et al.* (LIGO Scientific and Virgo Collaborations), Phys. Rev. Lett. **116**, 221101 (2016); **121**, 129902(E) (2018).
[5] M. Punturo *et al.*, Classical Quantum Gravity **27**, 194002 (2010).
[6] M. Maggiore *et al.*, J. Cosmol. Astropart. Phys. 03 (2020) 050.
[7] B. S. Sathyaprakash *et al.*, Bull. Am. Astron. Soc. **51**, 251 (2019), arXiv:1903.09221.
[8] V. Kalogera *et al.*, arXiv:2111.06990.
[9] R. P. Kerr, Phys. Rev. Lett. **11**, 237 (1963).
[10] E. T. Newman, R. Couch, K. Chinnapared, A. Exton, A. Prakash, and R. Torrence, J. Math. Phys. (N.Y.) **6**, 918 (1965).
[11] G. W. Gibbons, Commun. Math. Phys. **44**, 245 (1975).
[12] M. Zajacek and A. Tursunov, Observatory **139**, 231 (2019), arXiv:1904.04654.
[13] Y. Gong, Z. Cao, H. Gao, and B. Zhang, Mon. Not. R. Astron. Soc. **488**, 2722 (2019).
[14] R. D. Blandford and R. L. Znajek, Mon. Not. R. Astron. Soc. **179**, 433 (1977).
[15] V. Cardoso, C. F. B. Macedo, P. Pani, and V. Ferrari, J. Cosmol. Astropart. Phys. 05 (2016) 054; 04 (2020) E01.
[16] M. Zajaček, A. Tursunov, A. Eckart, and S. Britzen, Mon. Not. R. Astron. Soc. **480**, 4408 (2018).
[17] M. Zajaček, A. Tursunov, A. Eckart, S. Britzen, E. Hackmann, V. Karas, Z. Stuchlík, B. Czerny, and J. A. Zensus, J. Phys. Conf. Ser. **1258**, 012031 (2019).
[18] J. Preskill, Annu. Rev. Nucl. Part. Sci. **34**, 461 (1984).
[19] G. Bozzola and V. Paschalidis, Phys. Rev. Lett. **126**, 041103 (2021).
[20] D. Pereñiguez, Phys. Rev. D **108**, 084046 (2023).
[21] C. Dyson and D. Pereñiguez, Phys. Rev. D **108**, 084064 (2023).
[22] R. Xu, D. Liang, and L. Shao, Phys. Rev. D **107**, 024011 (2023).
[23] A. Stebbins and G. Krnjaic, J. Cosmol. Astropart. Phys. 12 (2019) 003.
[24] S. G. Ghosh and M. Afrin, Astrophys. J. **944**, 174 (2023).
[25] K. Akiyama *et al.* (Event Horizon Telescope Collaboration), Astrophys. J. Lett. **930**, L12 (2022).
[26] K. Akiyama *et al.* (Event Horizon Telescope Collaboration), Astrophys. J. Lett. **930**, L17 (2022).
[27] S. Vagnozzi *et al.*, Classical Quantum Gravity **40**, 165007 (2023).
[28] V. Ferrari and L. Gualtieri, Gen. Relativ. Gravit. **40**, 945 (2008).
[29] O. Dreyer, B. J. Kelly, B. Krishnan, L. S. Finn, D. Garrison, and R. Lopez-Aleman, Classical Quantum Gravity **21**, 787 (2004).
[30] E. Berti, A. Sesana, E. Barausse, V. Cardoso, and K. Belczynski, Phys. Rev. Lett. **117**, 101102 (2016).
[31] K. D. Kokkotas, Nuovo Cimento Soc. Ital. Fis. **108B**, 991 (1993).
[32] E. Berti and K. D. Kokkotas, Phys. Rev. D **71**, 124008 (2005).
[33] P. Pani, E. Berti, and L. Gualtieri, Phys. Rev. Lett. **110**, 241103 (2013).
[34] P. Pani, E. Berti, and L. Gualtieri, Phys. Rev. D **88**, 064048 (2013).
[35] Z. Mark, H. Yang, A. Zimmerman, and Y. Chen, Phys. Rev. D **91**, 044025 (2015).
[36] A. Zimmerman and Z. Mark, Phys. Rev. D **93**, 044033 (2016); **93**, 089905(E) (2016).
[37] H.-T. Wang, S.-P. Tang, P.-C. Li, and Y.-Z. Fan, Phys. Rev. D **104**, 104063 (2021).
[38] O. J. C. Dias, M. Godazgar, and J. E. Santos, Phys. Rev. Lett. **114**, 151101 (2015).
[39] O. J. C. Dias, M. Godazgar, J. E. Santos, G. Carullo, W. Del Pozzo, and D. Laghi, Phys. Rev. D **105**, 084044 (2022).
[40] O. J. C. Dias, M. Godazgar, and J. E. Santos, J. High Energy Phys. 07 (2022) 076.
[41] H.-T. Wang, P.-C. Li, J.-L. Jiang, G.-W. Yuan, Y.-M. Hu, and Y.-Z. Fan, Eur. Phys. J. C **81**, 769 (2021).
[42] G. Bozzola and V. Paschalidis, Phys. Rev. D **104**, 044004 (2021).
[43] P. K. Gupta, T. F. M. Spieksma, P. T. H. Pang, G. Koekoek, and C. V. D. Broeck, Phys. Rev. D **104**, 063041 (2021).
[44] C. A. Benavides-Gallego and W.-B. Han, Symmetry **15**, 537 (2023).
[45] C. García-Quirós, M. Colleoni, S. Husa, H. Estellés, G. Pratten, A. Ramos-Buades, M. Mateu-Lucena, and R. Jaume, Phys. Rev. D **102**, 064002 (2020).
[46] G. Carullo, D. Laghi, N. K. Johnson-McDaniel, W. Del Pozzo, O. J. C. Dias, M. Godazgar, and J. E. Santos, Phys. Rev. D **105**, 062009 (2022).
[47] R. Abbott *et al.* (LIGO Scientific, VIRGO, and KAGRA Collaborations), arXiv:2112.06861.
[48] H.-T. Wang and L. Shao, Phys. Rev. D **108**, 123018 (2023).

[49] B. P. Abbott *et al.* (LIGO Scientific and Virgo Collaborations), Phys. Rev. X **9**, 031040 (2019).
[50] R. Abbott *et al.* (LIGO Scientific and Virgo Collaborations), Phys. Rev. X **11**, 021053 (2021).
[51] R. Abbott *et al.* (KAGRA, VIRGO, and LIGO Scientific Collaborations), Phys. Rev. X **13**, 041039 (2023).
[52] B. P. Abbott *et al.* (LIGO Scientific and Virgo Collaborations), Phys. Rev. D **100**, 104036 (2019).
[53] R. Abbott *et al.* (LIGO Scientific and Virgo Collaborations), Phys. Rev. D **103**, 122002 (2021).
[54] S. A. Teukolsky, Astrophys. J. **185**, 635 (1973).
[55] E. Berti, V. Cardoso, and A. O. Starinets, Classical Quantum Gravity **26**, 163001 (2009).
[56] M. Isi and W. M. Farr, arXiv:2107.05609.
[57] C. W. Misner, K. S. Thorne, and J. A. Wheeler, *Gravitation* (W. H. Freeman, San Francisco, 1973).
[58] R. Cotesta, G. Carullo, E. Berti, and V. Cardoso, Phys. Rev. Lett. **129**, 111102 (2022).
[59] G. Carullo, W. Del Pozzo, and J. Veitch, Phys. Rev. D **99**, 123029 (2019); **100**, 089903(E) (2019).
[60] M. Isi, M. Giesler, W. M. Farr, M. A. Scheel, and S. A. Teukolsky, Phys. Rev. Lett. **123**, 111102 (2019).
[61] C. D. Capano, M. Cabero, J. Westerweck, J. Abedi, S. Kastha, A. H. Nitz, Y.-F. Wang, A. B. Nielsen, and B. Krishnan, Phys. Rev. Lett. **131**, 221402 (2023).
[62] H. Siegel, M. Isi, and W. M. Farr, Phys. Rev. D **108**, 064008 (2023).
[63] C. Shi, J. Bao, H. Wang, J.-d. Zhang, Y. Hu, A. Sesana, E. Barausse, J. Mei, and J. Luo, Phys. Rev. D **100**, 044036 (2019).
[64] E. Berti, V. Cardoso, and M. Casals, Phys. Rev. D **73**, 024013 (2006); **73**, 109902(E) (2006).
[65] H. Lim, G. Khanna, A. Apte, and S. A. Hughes, Phys. Rev. D **100**, 084032 (2019).
[66] A. Dhani, Phys. Rev. D **103**, 104048 (2021).
[67] A. Dhani and B. S. Sathyaprakash, arXiv:2107.14195.
[68] The LIGO Scientific Collaboration, the Virgo Collaboration, the KAGRA Collaboration, Report No. LIGO-P2100456, 2021, https://dcc.ligo.org/P2100456.
[69] G. Carullo, W. Del Pozzo, and J. Veitch, pyring (2023), https://zenodo.org/records/8165508.
[70] W. D. Pozzo and J. Veitch, https://github.com/johnveitch/cpnest (2015).
[71] J. Skilling, Bayesian Anal. **1**, 833 (2006).
[72] A. Freise, S. Chelkowski, S. Hild, W. Del Pozzo, A. Perreca, and A. Vecchio, Classical Quantum Gravity **26**, 085012 (2009).
[73] I. Kamaretsos, M. Hannam, and B. Sathyaprakash, Phys. Rev. Lett. **109**, 141102 (2012).
[74] S.-X. Yi, G. Nelemans, C. Brinkerink, Z. Kostrzewa-Rutkowska, S. T. Timmer, F. Stoppa, E. M. Rossi, and S. F. Portegies Zwart, Astron. Astrophys. **663**, A155 (2022).